

Environmental Science Advances

Accepted Manuscript

This article can be cited before page numbers have been issued, to do this please use: S. Javed, S. A. S. Chatha, S. Ali and A. Ullah, *Environ. Sci.: Adv.*, 2026, DOI: 10.1039/D6VA00121A.



This is an Accepted Manuscript, which has been through the Royal Society of Chemistry peer review process and has been accepted for publication.

Accepted Manuscripts are published online shortly after acceptance, before technical editing, formatting and proof reading. Using this free service, authors can make their results available to the community, in citable form, before we publish the edited article. We will replace this Accepted Manuscript with the edited and formatted Advance Article as soon as it is available.

You can find more information about Accepted Manuscripts in the [Information for Authors](#).

Please note that technical editing may introduce minor changes to the text and/or graphics, which may alter content. The journal's standard [Terms & Conditions](#) and the [Ethical guidelines](#) still apply. In no event shall the Royal Society of Chemistry be held responsible for any errors or omissions in this Accepted Manuscript or any consequences arising from the use of any information it contains.

Environmental Significance Statement

View Article Online
DOI: 10.1039/D6VA00121A

Increasing plastic waste and dye-contaminated wastewater are some of the major environmental issues. Upcycling of plastic waste into carbon dots for photocatalytic applications is a sustainable approach to waste management and water purification. This study has upcycled waste PET bottles into functional carbon dots and employed them in the photocatalytic degradation process of Reactive Black 5 dye. The Response Surface Methodology was used to determine the optimal operating conditions and increase degradation efficiency. The study also introduces a straightforward waste-to-value economic plan that can advance the circular economy objective and serve as a powerful method for treating dye-contaminated water.



Upcycling of PET-based plastic bottles into carbon dots for photocatalytic degradation of reactive black five using response surface methodology

Seemab Javed^{1,4}, Shahzad Ali Shahid Chatha^{1*}, Shafqat Ali^{2,3}, Aman Ullah^{4*}

¹Department of Chemistry, Government College University, Faisalabad-38000, Pakistan

²Department of Environmental Science, Government College University, Faisalabad-38000, Pakistan

³Department of Biological Sciences and Technology, China Medical University, Taichung 40402, Taiwan

⁴Department of Agricultural, Life & Environmental Sciences, University of Alberta, T6G 2G7, Canada

Correspondence:

Shahzad Ali Shahid Chatha

chatha222@gmail.com

Aman Ullah

ullah2@ualberta.ca

ABSTRACT

Water contamination and plastic pollution are the most prominent environmental issues, demanding state-of-the-art, sustainable remediations. This study describes the upcycling of waste polyethylene terephthalate (PET) bottles into carbon dots (CDs) and their application for the degradation of Reactive Black 5 (RB5) dye in water. CDs derived from PET were



successfully synthesized through a multistep green approach. Synthesized CDs were characterized for their structural, optical and surface features. UV–Vis revealed typical CD absorption behavior with an optical band gap of 3.14 eV. pH-dependent fluorescence spectra confirmed the presence of surface-state emission. FTIR, XRD, DLS, and AFM were consistent with the presence of surface functionalities and defects, surface-domain of disordered carbon materials, nanoparticles dispersion and CD-like morphology. Box–Behnken based Response Surface Methodology (RSM) models were established and optimum conditions were found by studying the effects of important operational parameters on RB5 degradation. The synthesized CDs exhibit a high removal rate of RB5 under light illumination (79.6-91.2%), whereas dark removal was relatively low (10.7-18.4%), which indicates that the major contribution came through light-driven processes, with the net photocatalytic degradation being high (68.9-72.8%). The RSM study established a region of optimal operation (pH = 7.4, CD dose = 0.50g/L, time = 75 minutes, and RB5 = 26mg/L). The response in the experiment was very similar to the predicted one, and this confirms the accuracy of the statistical optimization. PET-derived CDs offer an inexpensive, green, and efficient medium for dye-contaminated wastewater purification.

Keywords: Plastic Waste; Upcycling; Carbon Dots; Photocatalysis; Reactive Black Five

1. Introduction

Plastic pollution and industrial wastewater are two prominent environmental challenges of the modern era, causing widespread pollution and driving climate change^{1, 2}. Currently available strategies to address plastic waste-related issues, including mechanical recycling, incineration, and landfilling, have been reported with limitations³. Thus, the shortcomings of conventional techniques underscore the need to develop cutting-edge upcycling technologies to transform discarded plastic components into valuable, novel materials. Recently, various research studies have attempted to transform discarded polymeric



components into valuable carbon nanomaterials, such as graphene, carbon nanotubes and carbon quantum dots ⁴. Unlike mixed or composite plastics, the consistent chemical structure of PET, in which repeating units of terephthalate and ethylene glycol are linked, and its high carbon content make it an ideal candidate for transformation into valuable carbon-based nanomaterials ⁵. Its aromatic structure provides a strong foundation for forming graphitic networks of sp² hybridized carbon, while the polymer backbone contains oxygen groups that enhance the surface properties of the resulting carbon dots ⁶⁻⁹. PET bottles can be converted into activated carbon for the degradation of Brilliant Green dye, confirming the potential of plastic-waste-derived carbon dots in water treatment applications ¹⁰. Carbon dots represent a distinct class of zero-dimensional carbon-based nanomaterials with diameters usually smaller than 10 nm. Remarkable features of these particles, like chemical stability, low toxicity and photoluminescence, make them attractive for multiple applications. In terms of structure, the particles comprise a graphitic structure with a large amount of sp² bonds, together with surface groups containing oxygen atoms ^{11, 12}. These characteristics make them excellent candidates for environmental applications, including metal removal, degradation of organic contaminants, and biosensing ¹³. In parallel, textile wastes containing high levels of recalcitrant colorants, which pose significant health and ecological hazards and are not easily treatable ¹⁴. One of the common reactive azo dyes is Reactive Black 5 (RB5), which is particularly recalcitrant due to its complex structure, aromaticity, and stability, necessitating a sustainable strategy for its removal from waterbodies ^{15, 16}. Despite extensive research the existing dye-treatment methods are not up to the mark, as physical adsorption can relocate contaminants instead of destroying them and might produce secondary waste; biological treatment may be sluggish and susceptible to inhibitory effluent matrices, and chemical oxidation/coagulation may need a substantial number of reagents and may need rigid

View Article Online
DOI: 10.1039/D6VA00121A



control of pH yet still experience incomplete mineralization of complex wastewater. 14/View Article Online
DOI: 10.1039/D6VA00121A

Photocatalysis represented as a promising approach, recent research has highlighted the need for environmentally friendly materials for the removal of dyes from wastewater. Effective photo assisted degradation of wastewater dyes using CdS nanoparticles trapped in porous g-C₃N₄/SiO₂ composites, showing the importance of engineered photocatalysts for the removal of organic dyes¹⁷. A calcium alginate–polydopamine biocomposite for sustainable removal of Brilliant Green dye indicates the growing interest in greener adsorbent systems for dye remediation¹⁸. Efficient photocatalytic systems are still largely developed with hybrid and chemical synthesis. Meanwhile, the conversion of urban and plastic waste is increasingly recognized as a key approach to sustainable environmental management, but further valorization strategies are needed to create functional materials¹⁹. In this context, carbon dots (CDs) have become popular low-toxicity, tunable, and photostable nanomaterials, which can serve as photocatalysts, especially in visible light, to achieve water treatment in the real world²⁰. Recent studies demonstrate that carbon-dot nanomaterials are promising in photo/electrocatalytic removal of organic pollutants, owing to their photoresponsive features, functionality and charge carrier transfer²¹. In this regard, this project upcycling plastic waste into carbon dots and their applications for photocatalytic degradation of RB5 addresses problems in a single integrated process. This two-fold solution connects the plastic waste management with wastewater treatment directly, and takes advantage of the fact that CD semiconductor systems can be used to amplify light absorption and charge transfer to accelerate the degradation of dyes²². In photocatalysis, interacting variables are important to process performance; hence, Response Surface Methodology (RSM), particularly Box-Behnken Design (BBD), can be a good choice to model the nonlinear nature of process performance and determine the real optima with fewer experiments compared to one-factor-at-a-time tests^{23, 24}. Overall, this



study focuses on the synthesis of plastic-based carbon dots, which can be regarded as a viable platform for the photocatalytic elimination of RB5 and RSM-BBD, thereby optimizing working conditions and achieving maximum degradation efficiency and feasibility. The most significant future directions are also expected to include performance validation on real textile wastewater across more water chemistries, catalyst recovery/reuse, and long-term photostability, performance, and integration into the optimized process in continuous-flow or sunlight-driven reactors.

View Article Online
DOI: 10.1039/D6VA00121A

2. MATERIALS AND METHODS

2.1 Chemicals and reagents

In this study, a sustainable approach was applied, and no harsh chemicals were used for the preparation. In the dye degradation study, only hydrochloric acid (HCl, analytical grade, Merck, Germany) and sodium hydroxide (NaOH, analytical grade, Sigma-Aldrich, USA) were used to adjust the pH.

2.2 Pre-treatment of Polyethylene terephthalate (PET) based plastic waste

Polyethylene terephthalate (PET) waste bottles were collected from the cafeteria of Government College University, Faisalabad, Pakistan. Over a period of one month, discarded PET bottles were collected manually, illustrating the extensive consumption of bottled water and ensuring a continuous supply of PET waste. These bottles were sorted by color and labeling to minimize contamination risk. Only transparent PET bottles with specific colors and coatings were used to ensure contamination-free samples, as such features can affect the quality and composition of the carbon dots. The PET bottles were thoroughly cleaned and dried at room temperature, then first washed with tap water, then with distilled water, and finally dried to remove all soluble contaminants²⁵. The bottles were then dried at room temperature and shredded into small pieces using a mechanical



shredder. The shredded sample was dried at 60 °C for 12 hours in a heating oven (NR-38XDG, JW-Enviro) and stored in a polyethylene zipper bag for further experiments. View Article Online
DOI: 10.1039/D6VA00121A

2.3 Synthesis of CDs

In the calcination stage, a starting material, 3.0 g of pre-treated PET, was poured into a ceramic crucible and heated in a muffle furnace (B-170 (Nabertherm)) for 5 hours at 500 °C. Thermal treatment of PET results in carbonized material. After calcination, the carbonized PET is cooled to ambient temperature (25 °C) to avoid rapid structural changes from thermal shock. Then, 50 mL of deionized water is added to extract the carbon dots, thereby aiding their dispersion. The calcined product was a blackish-brown powder that was sieved through a 0.21 mm screen, and larger particles were removed using an electric mortar and pestle. The fine powder was added to a solution of distilled water and stirred thoroughly at room temperature for 24 hours under appropriate conditions. This stirring was used to achieve uniform dispersion of carbon nanoparticles. Hydrothermal treatment at 180 °C was conducted in a sealed Teflon-lined autoclave for 6 hours. This process breaks down polymer chains into carbon-rich particles, converting the plastic into carbon dots, as previously reported²⁵. The obtained crude carbon dots (CDs) solutions were sonicated for 30 minutes for 100W at 25 °C to ensure proper dispersion of any formed clumps. The purpose of sonication was not only to break up agglomerates but also to modify the surface functional groups of the CDs and facilitate dopant incorporation²⁶. The yield of carbon dots was calculated using the mass ratio of the manufactured product to the initial plastic waste sample as reported in the previous studies²⁵.

$$Y\% = \left(\frac{\text{Mass of CDs product}}{\text{Mass of plastic waste sampled}} \right) \times 100$$



In this study, when 10 grams of PET-based carbonized material were processed, approximately 4.8 grams of CDs were recovered, yielding 48.16%. The synthesis process is shown in Supplementary Fig S1-S3.

View Article Online

DOI: 10.1039/D6VA00121A

2.4 Characterizations of Carbon Dots

The physicochemical characteristics, surface chemistry, and dispersion behavior of the synthesized carbon dots were analyzed using spectroscopic analysis, particle size analysis, and thermal analysis. A UV -visible spectrophotometer (Shimadzu UV-1800, Japan) was used to measure the absorption spectrum of the CDs between 200 and 800nm. It was measured in quartz cuvettes with a 1 cm path length, using deionized water as the blank. The photoluminescence (PL) was measured with a spectrofluorometer (Shimadzu RF-6000, Japan). The excitation wavelengths ranged from 300 to 420 nm, and the monitored wavelengths ranged from 350 to 650 nm. The fluorescence performance of the CDs under excitation was analyzed to determine emissive properties arising from surface states. The influence of pH on the fluorescence properties of the CDs was studied by varying the pH of aqueous CD solutions from 2 to 12 using dilute hydrochloric acid (HCl) and sodium hydroxide (NaOH) solutions. Fluorescence stability was compared at a constant excitation wavelength under the same instrumental conditions. A dynamic light scattering analyzer (Malvern Zetasizer Nano ZS, UK) was used to identify the hydrodynamic particle size distribution of the CDs at room temperature. Fourier-transform infrared (FTIR) spectroscopy (Bruker Tensor 27, Germany) over the wavenumber range 4000-400 cm^{-1} was used to characterize the surface functional groups and chemical bonding of the synthesized CDs. X-ray diffraction (XRD) (PANalytical XPert PRO, Netherlands) was used to probe the crystalline architecture of the CDs using Cu $K\alpha$ radiation (1.5406 Å). Diffraction patterns were measured over a 2θ range of 10-80 °, allowing evaluation of the degree of crystallinity and carbonaceous structural order in the CDs. Atomic force microscopy

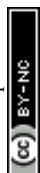


(AFM) was used to investigate the topographical morphology and height of the carbon dot (CD) particles. A dilute CD dispersion was drop-cast onto a cleaned, wave-cleaved mica substrate, allowed to adsorb, gently rinsed with ultrapure water to remove residual, then dried under a stream of nitrogen at room temperature, and finally imaged. Topography was acquired at ambient conditions in tapping mode using an AFM system (Shimadzu WET-SPM 9600, Shimadzu, Tokyo, Japan).

2.5 Photocatalytic application of synthesized CDs

Reactive Black 5 is extensively used in textile dyeing and is commonly detected in colored textile effluents. The azo ($-N=N-$) linkage and aromatic structure of RB5 make it chemically stable and recalcitrant, which ultimately disturbs the environmental balance²⁷. In this regard, RB5 is selected for this study to evaluate the degradation potential of PET-derived carbon dots. All the solutions were prepared diluted with deionized water (DI), and (0.1M) HCl/NaOH solutions were used for the adjustment of pH. The stock solution of dye (1000 mgL^{-1}) was prepared in the dark. Then, working solutions were prepared by dilution to the corresponding initial concentration (C_0). The concentrations were evaluated by UV-Vis spectroscopy (Lambda 25, PerkinElmer) at their maximum absorbance (λ -max). The absorbance-to-concentration conversion was performed by constructing a calibration curve, as shown in Fig S4 and Table S1. A bath reactor with a borosilicate beaker was used for photocatalytic experiments, with a working volume of 100 mL and continuous stirring to maintain a homogeneous suspension. A UV-Vis lamp (Shimadzu UV-1800, Japan) was used as the irradiation source and maintained a constant distance throughout all experimental trials to maintain a uniform photon flux.

The designed dosage of CDs (g/L) was added prior to irradiation. Each experimental trial was stirred in the dark for 30 minutes before irradiation to establish adsorption-desorption equilibrium, which is required to evaluate adsorption-dependent dye removal and to



address the overestimation of CDs photocatalytic ability. Photocatalysis starts by switching the light source on at time (t=0). After a predetermined time, aliquots were centrifuged and analyzed by UV-Vis spectroscopy. The confirmation experiments of the photocatalytic and adsorption potential were performed before the optimization of reaction conditions. The following equation was used to calculate the dye removal % from synthetic wastewater.

$$\text{Dye removal \%} = \frac{C_0 - C_t}{C_0} \times 100$$

The concerned reaction parameters (pH, CDs dosage, irradiation/contact time, and initial RB5 concentration) were evaluated, and the BBD model was evaluated using replicate central points. The reaction conditions were optimized using Response Surface Methodology (RSM) based on a Box–Behnken design (BBD) with the following factors as described in Table S2 of supplementary file:

Table 1: RSM (BBD) based experimental design for photocatalytic degradation of RB5

Run	A: Carbon dots dose (g/L)	B: Dye conc. (mg/L)	C: pH	D: Time (min)	RB5 Degradation (%)
1	0.8	30	8	30	68.5
2	0.5	30	5	30	50.2
3	0.8	30	8	120	96.4
4	0.8	30	11	75	87.6
5	0.2	30	11	75	70.8
6	0.5	50	8	30	44.7
7	0.5	30	11	30	55.9
8	0.8	30	5	75	76.1
9	0.5	10	5	75	82.7
10	0.5	30	8	75	88.4
11	0.2	30	8	30	46.8
12	0.2	30	8	120	86.9
13	0.2	10	8	75	84.5
14	0.5	10	8	30	63.8
15	0.8	10	8	75	95.1
16	0.5	30	11	120	92.8
17	0.5	30	8	75	87.6
18	0.5	30	5	120	88.9
19	0.5	10	11	75	88.6
20	0.5	50	11	75	78.9
21	0.5	30	8	75	89.1
22	0.2	50	8	75	66.7
23	0.5	30	8	75	88.0
24	0.5	50	8	120	90.3
25	0.5	10	8	120	95.0
26	0.8	50	8	75	84.2
27	0.5	30	8	75	87.9



28	0.5	50	5	75	74.6
29	0.2	30	5	75	61.9

View Article Online
DOI: 10.1039/D6VA00121A

Experimental data were fitted in a second-order (quadratic) response surface model with 4 factors (A, B, C, D). Time-resolved RSM-predicted data were further quantified to evaluate the kinetics under the optimized conditions and to determine the rate constant and half-life.

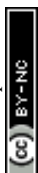
Reusability potential of carbon dots

The investigation of the recyclability of the CDs as a photocatalyst for RB5 degradation was carried out under the optimal photocatalytic conditions for five consecutive runs. At the end of each photocatalytic degradation cycle, the reaction suspension was centrifuged (8000 rpm, 10 min) to separate the photocatalyst from the reaction mixture. The recovered photocatalyst was washed several times with distilled water and ethanol to get rid of the adsorbed dye molecules and intermediate products formed during the degradation process. After washing, it was dried in an oven at 60 °C for 6 h and then reused for the next cycle by adding it to a fresh dye solution with the same concentration. The entire experiments of catalyst reuse were conducted under identical photocatalytic to investigate its stability and reusability. The photodegradation efficiency was then determined by UV-Vis study of RB5 before and after exposure to light.

2.6 Statistical analysis

All preliminary calculations were performed in Microsoft Excel, and the graphical presentations were created in Origin Pro 2020. Optimizations and statistical modeling by RSM (BBD) were performed with Stat-ease Design-Expert 360, where the fitting of quadratic regression models and evaluation of ANOVA ($p < 0.05$), including coefficient significance, lack of fit testing, and fit material's goodness (R^2 , adjusted R^2 , predicted R^2), supported by actual vs predicted plots and residual diagnostics. Three replicates were measured in all experiments, and results were reported as mean \pm standard deviation (SD).

3. RESULTS AND DISCUSSION



This study is designed to link the synthesis of carbon dots (CDs) with their structure-property relationships and ultimately apply them to degrade Reactive Black 5 (RB5). The optimal formation of CDs and their main physicochemical characteristics are initially verified by the optical (UV -Vis, PL/fluorescence, pH-dependent fluorescence), chemical (FTIR), structural (XRD), colloidal (DLS), and morphological (AFM) characterization. Based on these results, the performance of the CDs in photocatalytic degradation of RB5 is then interpreted, including the effects of operational variables. Response Surface Methodology (RSM) is used to model and optimize the efficiency of the material, determine the effect of interactions between the factors, and identify optimal conditions to achieve maximum results, which is assisted by statistical diagnostics and validation experiments.

3.1 Photophysical and optical characteristics of CDs

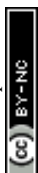
The UV/Vis absorption spectra of CDs showed typical features of well-structured carbon nanomaterials, aligning with previous findings.²⁸ The spectrum shown in Figure 1 features two prominent absorption bands: a sharp peak at 265-270 nm and a broad band at 340-360 nm. The first peak indicates π - π^* transitions caused by the aromatic nature of sp^2 -hybridized regions in the synthesized carbon dots. The second, broader band corresponds to n - π^* transitions, typically associated with carbonyl (C=O) or other oxygen- or nitrogen-based functional groups on the CD surface. These two traits demonstrate significant surface functionalization, which is crucial for explaining CD fluorescence and reactivity. These findings are consistent with the reported literature^{29,30}. The data of the UV-vis absorbances were then converted to the absorption coefficient ($ah\nu$), and a plot of $(ah\nu)^2$ vs photon energy ($h\nu$) was drawn as the direct Tauc plot, as shown in Figure 2. The linear span around the absorption edge is extrapolated to ($E_g = 3.14$ eV), indicating permitted electronic

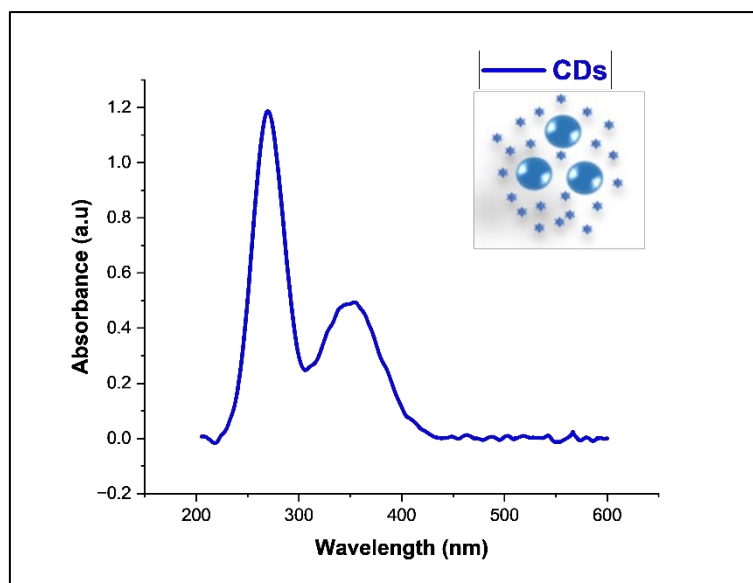
View Article Online
DOI: 10.1039/D6VA00121A



changes in the sp^2 domains/surface states of the CDs. This energy range generally facilitates efficient radiative recombination and is expected to exhibit excellent fluorescence. View Article Online
DOI: 10.1039/D6VA00121A

The photoluminescence characteristics of the CDs were analyzed using fluorescence emission spectroscopy. The excitation wavelengths range from 280 to 340 nm, with the fluorescence emission spectra shown in Figure 3. All wavelengths exhibit emission peaks between 420 and 480 nm, with the strongest at 280 nm. This intense blue fluorescence signals the presence of aromatic and carbonyl groups on the surface, which are known to promote $\pi-\pi$ and $n-\pi$ transitions in carbon dots³¹. The emission peak shifts toward the red spectrum, while the emission intensity reduction can be attributed to multiple surface states and diverse particle sizes that form traps with different emissions spectra. A red shift and decreased intensity at an excitation of 340 nm indicate the presence of heterogeneous emissive sites on the CDs. This trend aligns with previous studies showing excitation-dependent blue emission of biomass waste-derived CDs, with a strong signal at 450 nm. The current analysis indicates that emissions are high at low excitation levels, likely due to the polymeric polyethylene terephthalate's extended aromatic-conjugated system. The pH-dependent fluorescence property of carbon dots (CDs) is an essential feature, especially for environmental monitoring³². Figure 4 shows that the fluorescence intensity of carbon dots varies widely across different pH values, indicating a significant impact of pH on their function. At lower pH values (pH 2-4), the fluorescence intensity remains relatively low because the surface functional groups, such as $-\text{COOH}$, $-\text{OH}$, and $-\text{NH}_2$, go protonated, which disrupts electronic conjugation and quenches fluorescence³³. As the pH rises from 6 to 12, fluorescence intensity increases accordingly, suggesting deprotonation and stabilization of surface states that support radiative recombination of excited electrons. This observed behavior matches previous research on carbon³⁴.





View Article Online
DOI: 10.1039/D6VA00121A

Figure 1: UV–Vis spectrum of carbon dots showing a strong peak at around 280 nm and a secondary band near 350 nm. The observed transitions suggest π – π^* and n – π^* electronic transitions of carbon dots

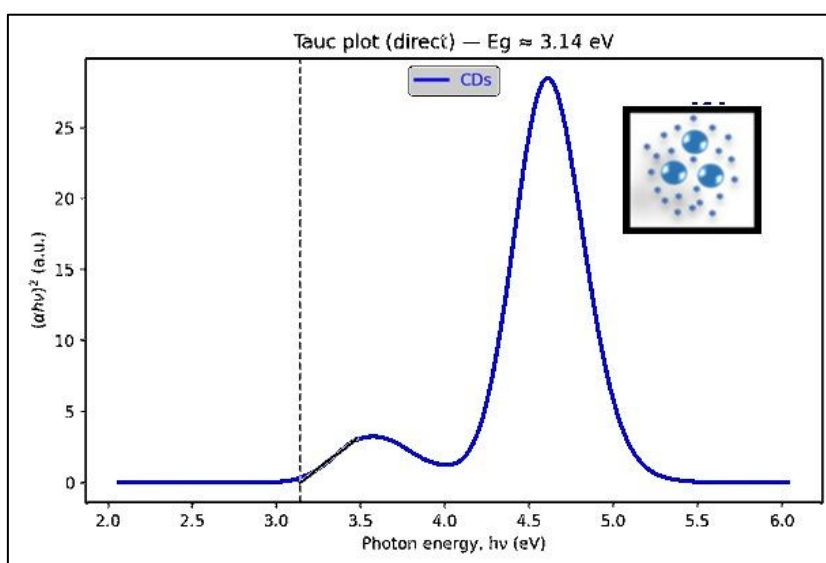
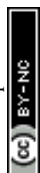


Figure 2: Direct Tauc plot, $(ahv)^2$ vs. photon energy (hv). The linearity of the absorption edge was estimated from the results, and $(ahv)^2$ was extrapolated to zero.



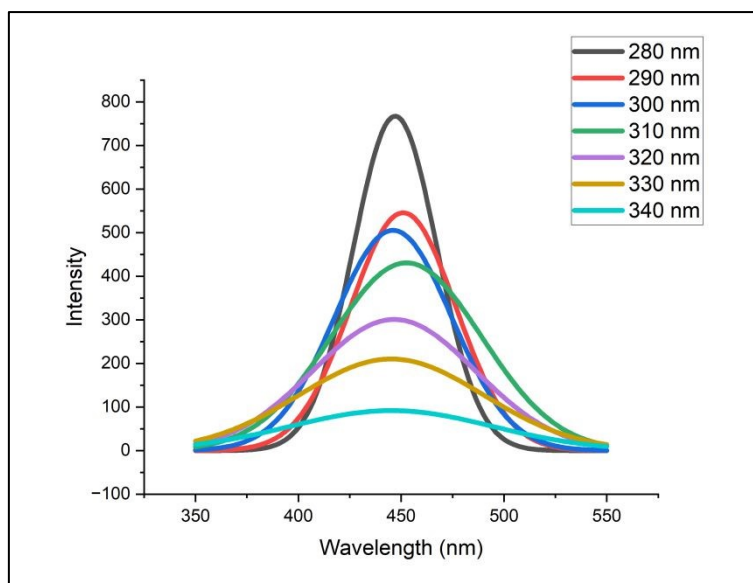


Figure 3: Fluorescence emission spectra of carbon dots at different excitation wavelengths (280–340 nm).

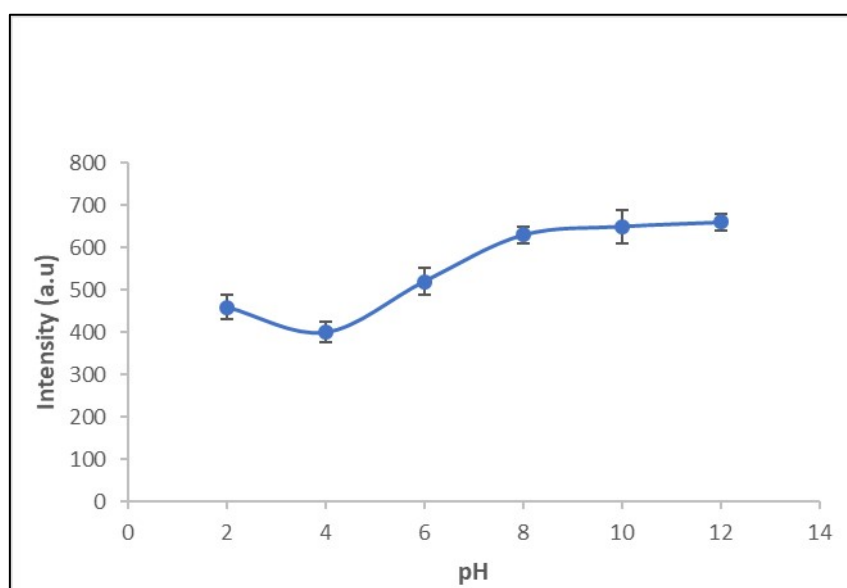


Figure 4: The pH-dependent variation in the fluorescence emission intensity of carbon dots

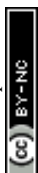
3.2 Physicochemical, Structural, and Morphological Analysis

Carbon dots (CDs) are gaining global recognition for their advanced optical, electrical, and biocompatible properties³⁵. Figure 5 illustrates the effect of dynamic light scattering (DLS)



on CDs and the distribution of the hydrodynamic diameters of the particles. The percentage of particles, as well as the emergence of a significant peak in the particle size distribution, imply that most of the grown CDs are within a given range of dimensions, indicating homogeneous properties quite well. The presence of only one sharp peak indicates a single dispersant (monodisperse), meaning the dispersants are relatively uniform in size. In contrast, the presence of multiple peaks or a broad distribution suggests polydispersity, as reported earlier³⁶. DLS measurements tend to report a hydrodynamic diameter larger than the CD's actual core size. This difference arises from hydration layers and surface functional groups that interact with solvent molecules³⁷. The hydrodynamic size of CDs with hydrophilic functional groups, such as -OH and -COOH, is larger due to the solvation effect³⁸. A prominent single peak with an estimated size of 5–12 nanometers was observed based on DLS spectra. This indicates that the carbon dots are very tiny and fall within the expected range of quantum-sized nanomaterials. Additionally, the absence of secondary peaks in the graph suggests there are no large particles or major aggregates in the sample. This implies that the carbon dots are evenly dispersed throughout the solution and that the preparation method effectively prevents particle clumping or uneven size distribution. This monodisperse size distribution is crucial in applications where uniform particle size is critical to performance and stability in biological or environmental systems, such as bioimaging, drug delivery, and photocatalysis.

The FTIR spectrum in Figure 6 shows prominent peaks corresponding to hydroxyl (-OH), carboxyl (-COOH), carbonyl (C=O), and aromatic C=C groups, indicating successful oxidation and functionalization. The presence of hydroxyl groups was indicated by a broad absorption band at 3200-3500 cm^{-1} , corresponding to O-H stretching vibrations. These hydroxyl groups make the CDs more hydrophilic and soluble in water. The presence of carboxyl groups and those formed during PET oxidation was identified by a strong



absorption peak around 1700 cm^{-1} . A signal around 1600 cm^{-1} indicates C=C stretching vibrations, suggesting that aromatic carbon structures in their sp_2 form are still partially preserved in the PET precursor. The stretching of C-O vibrations between 1100 and 1300 cm^{-1} is the reason why the observed peaks suggest the presence of ether functionalities. The decreased absorption between 600 - 900 cm^{-1} is related to aromatic C-H bending and is demonstrated by the presence of retained aromatic rings, as indicated by earlier research ³⁹, ⁴⁰. The broad peak of OH/NH in the 3200 - 3500 cm^{-1} region indicates that the CDs contain many hydrophilic groups, which increase their water solubility and enhance their fluorescence. This has been observed in earlier studies of CDs prepared from biomasses like glucose or orange peel, and high hydrophilicity has been closely associated with quantum yield ⁴¹.

PET is inherently aromatic, but when converting to CDs, some of its aromatic nature is preserved, as shown by the C=C skeletal vibrations around 1600 cm^{-1} . Conversely, the loss of ester peaks and the emergence of new functional group signals are major structural changes. This demonstrates that the CDs are entirely new nanostructures formed through a controlled transformation rather than through conventional PET grinding. It has been established that the luminescent behavior of CDs depends on observed FTIR peaks of hydroxyl, amine, carboxyl, and aromatic groups. These groups can facilitate radiative recombination by acting as both electron acceptors and donors. According to the literature, these surface groups play a key role in regulating PL emission. PET-based CDs exhibit FTIR spectra similar to those of CDs derived from natural waste materials such as fruit peels or paper, and their natural polymer backbone confers a slight aromatic character ⁴².

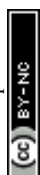
The XRD spectrum of Polyethylene Terephthalate (PET) is shown in Figure 7, with a strong diffraction peak at $2\theta = 16.5$. The origin of this sharp peak represents the semi-crystalline nature of PET, corresponding to the (010) plane of its triclinic crystalline structure. This



high crystallinity in the raw PET material produces a sharply defined, intense peak. The lack of extra sharp peaks suggests there are no multiple crystalline phases, which is common in commercial PET. By contrast, the XRD pattern of PET-derived Carbon Dots (CDs). The prominent peaks in the diffraction pattern at 2-theta values of 26.0, 30.5, 38.0, and 43.8 degrees indicate a significant structural change in the initial PET material after the three treatments. The width of numerous peaks suggests the formation of a nanocrystalline carbon framework, typical of carbon dots produced by heating or degrading polymeric precursors, as reported in the literature^{43, 44}.

The presence of a broad, diffuse peak near $2\theta = 22.6$ degrees indicates an arrangement of graphitic carbon domains. The peak at 22.6° corresponds to the (002) diffraction peak of graphitic carbon; however, it is notably broader due to the nanoscale roughness of the CDs. The (002) plane of graphitic carbon, which is observed to have the highest value of 26° , indicates that the graphitic or sp^2 hybridized structure of carbon is present in the CD core. The interlayer spacing (d-spacing) in this research is calculated using Bragg's Law and found to be greater than that of crystalline graphite ($d_0 = 3.34 \text{ \AA}$), confirming the presence of disordered graphitic layers, which directly affects their optical and electrical properties. The combination of sp^2 and sp^3 domains creates a structurally diverse carbon network, thereby increasing photoluminescence and enabling variable bandgap behavior. These findings align with the existing literature, which shows that the overall XRD features of carbon dots indicate short-range order and a relatively high degree of disorder when produced from waste polymers, plastic materials, or other polymers^{45, 46}.

AFM micrographs ($10 \times 10 \text{ \mu m}$ scan area) clearly demonstrate that the nanoscale carbonaceous domains are dispersed on a smooth matrix. The maximum vertical scale is 30,15nm as indicated in the 3D image in Figure 8 and 9, while the topographic scan ($R_a \approx 2.03 \text{ nm}$; $R_q \approx 3.71 \text{ nm}$; $R_z \approx 92.45 \text{ nm}$; $R_p \approx 76.98 \text{ nm}$; $R_v \approx 15.47 \text{ nm}$) extracted by the



statistical roughness parameters, shows the distribution of nanoscale protrusions across the scanned surface. A homogenous nanostructure is identified with the low average roughness (2nm), which indicates the formation of nano-range carbon domains consistent with carbon dots, which is further supported by the line profile analysis (A-B) and (C-D). The nanoscale peaks of the height profile reveal sub nanometer to a few (0.4-1.9) range with localized higher protrusions, which indicates the presence of spherical carbon dots with some graphene-like layers. AFM heights commonly fall in the 1-5nm range with respect to 2-6 nm, embedded in graphene layers, which mostly depend upon the synthesis conditions and post-treatment protocols⁴⁷. The elongated and interconnected framework of carbon, which is induced by calcination followed by hydrothermal treatment and formation of oxidation. Further exfoliation and dispersion of clusters into smaller carbon dots occur with subsequent sonication. A fragmentation-assisted reduction in size is also reported for plastic waste-derived carbon dots in previous studies, where dispersion is improved and particle stacking is reduced by post-treatment sonication³⁴. The AFM results of this study show nanoscale profiles having vertical dimensions which is aligned well with the previously reported thickness (1-10 nm) of carbon dots²⁷. It indicated that the synthesized carbon dots are not residues of bulk carbon but rather nanoscale dots. The AFM images showed that the surface of carbon dots was rugged and nanostructured with a difference of 30.15 nm. This provides greater surface area for the adsorptions of RB5, light absorption and generation of ROS, and hence enhancing photocatalytic degradation.

SEM images of a sample taken at different magnifications reveal that the surface morphology is rough, fragmented, solid, and carbonaceous, with small dot-like granular particles randomly dispersed on the surface. Carbon dots appear to be an irregular, carbon-rich matrix formed post-carbonization, with fine, bright particulate domains attached to the surface at higher magnification (b-d). These particles are aggregated carbon dots on the



surface of the carbonaceous material. The aggregation of carbon dots happens because of surface functional groups and extremely small nanoscale dimensions that can lead to aggregation during the drying process. The existence of these dot-like carbonaceous particles on the solid carbonaceous matrix confirms successful formation of carbon dots⁴⁸.

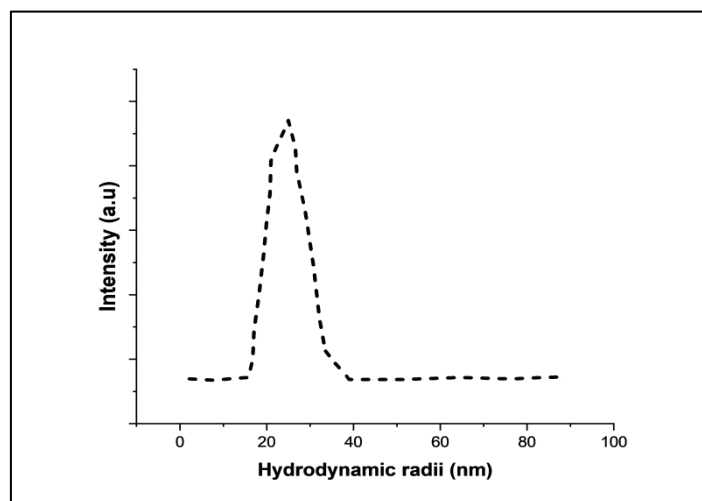


Figure 5: DLS spectrum of carbon dots indicating a large dimension of the average particle size distribution with a significant peak of 25 nm hydrodynamic radius

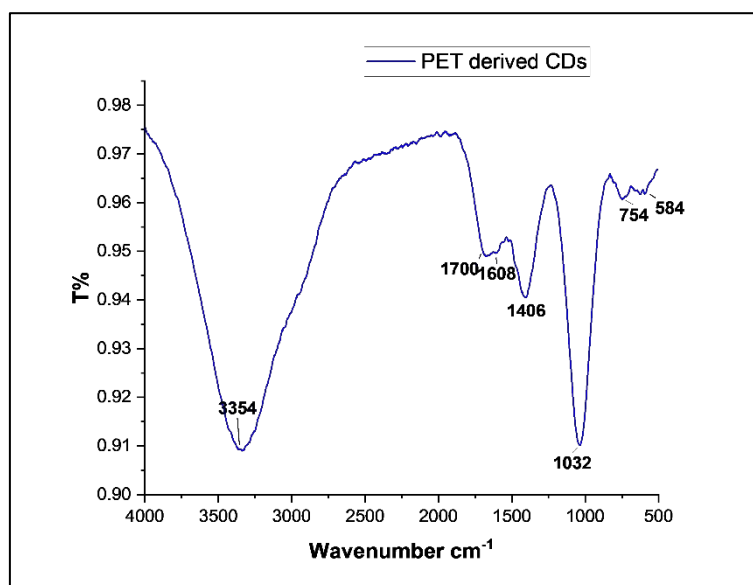


Figure 6: FTIR spectrum of synthesized carbon dots.



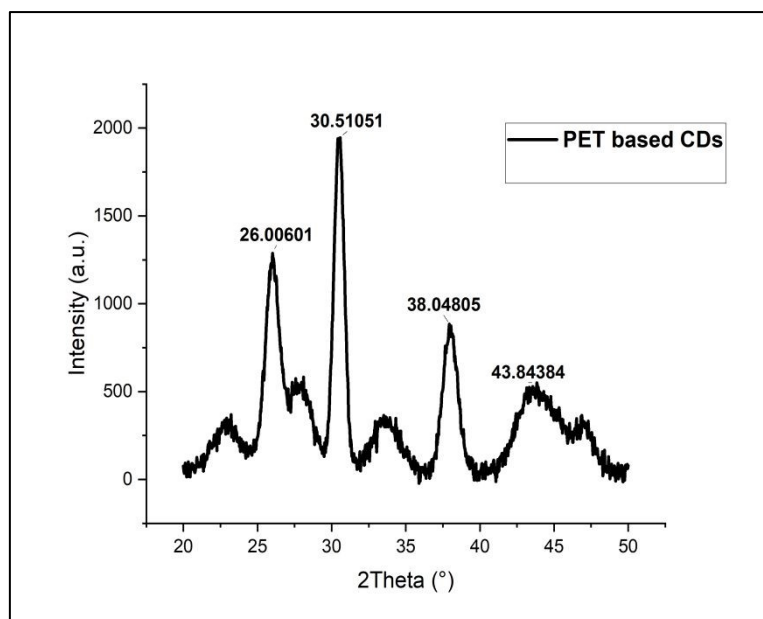


Figure 7: XRD analysis of PET-derived CDs

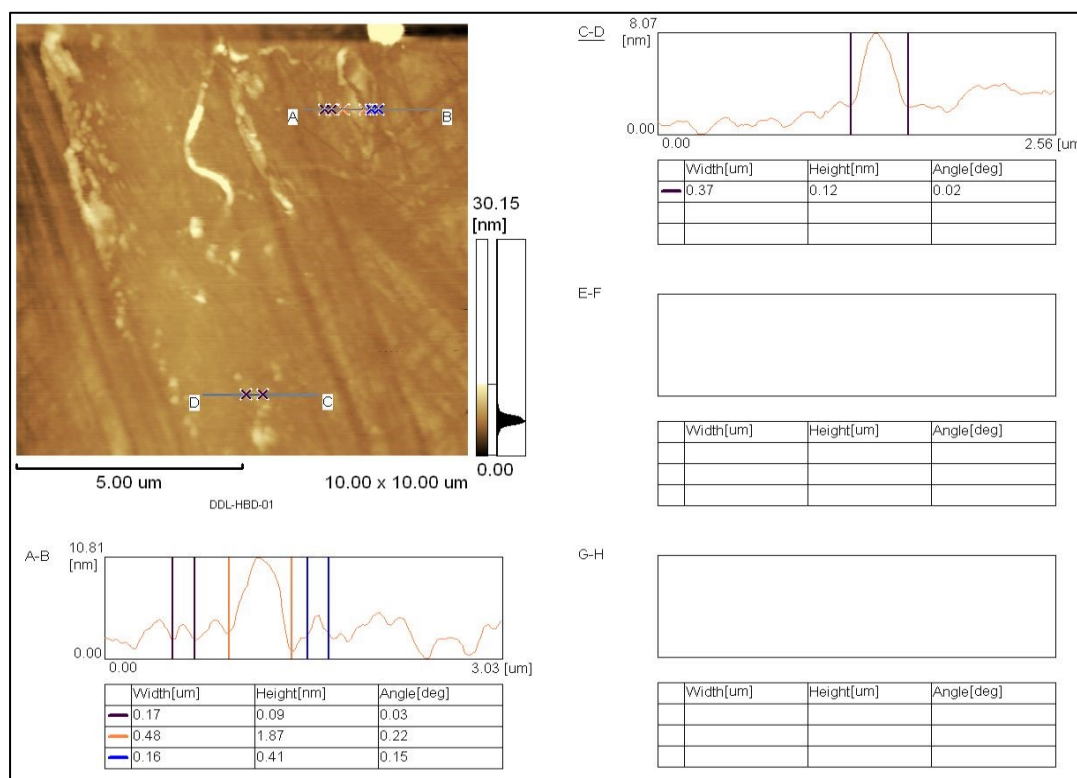


Figure 8: AFM topography and height profile of carbon dots (CDs). The surface morphology revealed in the 2D AFM height image (scan size 10.00 x 10.00 mm, scale bar 5.00 mm) with the highest and lowest height being 0 and 30.15 nm respective.



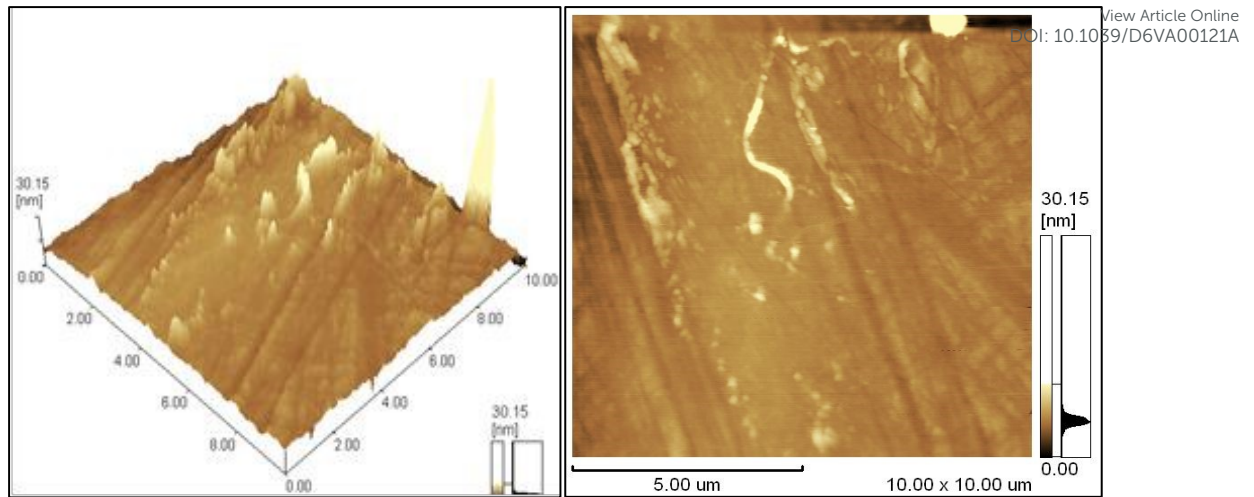


Figure 9: AFM images of 3D surface topography of CDs deposited over a $10 \times 10 \mu\text{m}$ scan area on the substrate (height scale 0–30.15 nm)

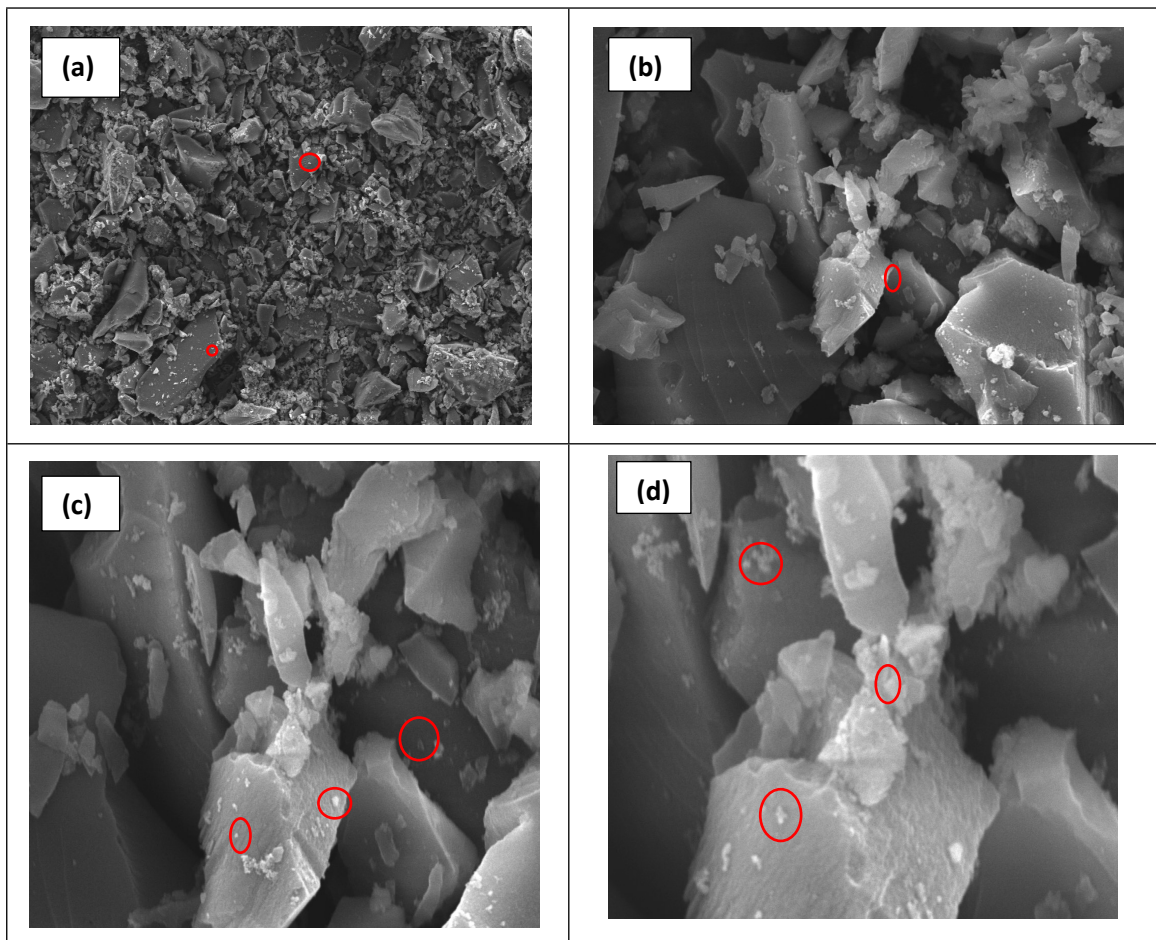
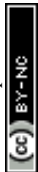


Figure 10: SEM micrographs of synthesized carbon dots deposited on solid carbonaceous surface; (a) 1k magnification, (b) 10k, (c) 30k and (d) 40k.

3.3 Applications of CDs for RB5 degradation



PET-derived carbon dots were studied for their adsorption and photocatalytic degradation potential. The differentiation of both phenomena was analyzed through controlled and confirmatory experiments to understand the actual degradation assisted by CDs. The dye-removal process was further optimized using RSM (Box–Behnken design) to determine the optimal operational window.

3.3.1 Quantification of dark adsorption vs. photocatalysis

The dark adsorption equilibrium was established for 30 minutes before each photocatalytic experiment, separating dye removal by adsorption from photocatalysis and preventing overestimation of photocatalytic behavior. In general, increasing the adsorbent dose increases the adsorption rate due to more surface sites and stronger electrostatic and π - π interactions between the adsorbent's functional groups and the dyes⁴⁹. While a single adsorption mechanism in the presence of light is insufficient for total dye removal, this indicates the presence of a light-mediated pathway^{50, 51}. The light removal (%) is the sum of the RB5 removal at the conclusion of adsorption + photocatalysis. All runs show a high percentage of light removal, indicating that the additional pathway is another dominant, activated by light in the presence of adsorption. The maximum light removal of 91.2 % was at pH 8, a CDs dose of 0.50 g/L, RB5 = 20 mg/L, and 65 min, indicating that this condition provides good catalytic activity or good adsorption-reaction coupling, but in-depth optimization can be achieved through statistical methods. In this study, a quadratic RSM model is employed. A pre-optimization baseline summary of the experimental data is presented in Figure 10, and the explanatory data are included in the supplementary file as Table S2.



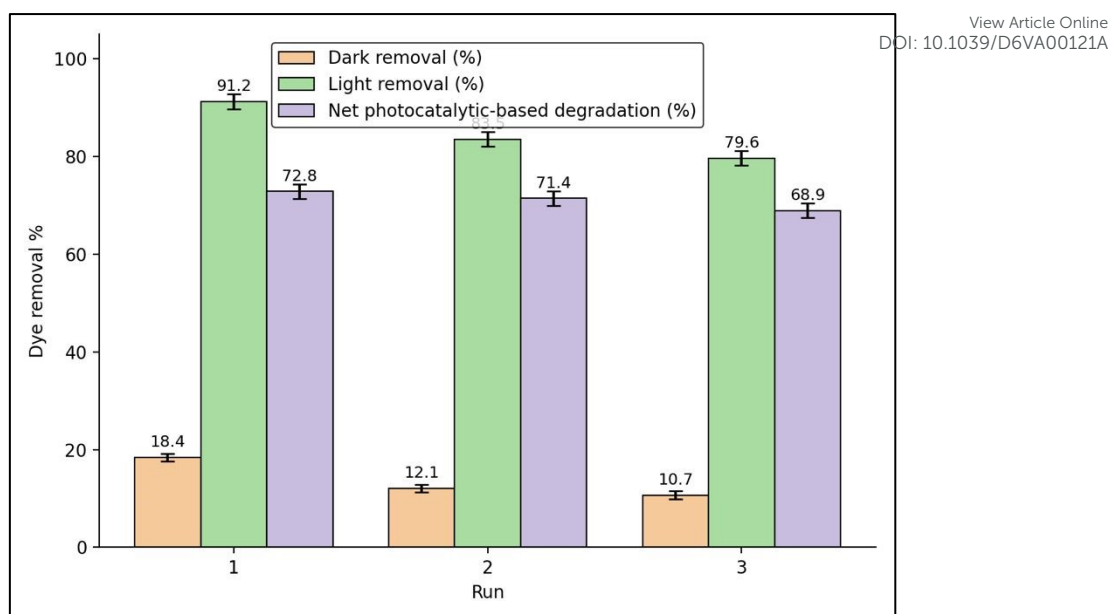


Figure 11: Analysis of RB5 removal potential via dark adsorption, light removal, and net photocatalytic degradation

3.3.3 RSM-based optimization of dye degradation phenomenon

As seen in Figure 12A, the RB5 degradation efficiency increases significantly with increasing CDs dose ($0.2\text{--}0.8\text{ gL}^{-1}$) and with increasing pH towards the alkaline pH range. The optimum degradation is predicted in the high-dose/high-pH area, particularly at 0.8 g L^{-1} CDs and pH 11, under fixed RB5 concentration of 30 mg L^{-1} and irradiation time of 75 min. The influence of pH implies that RB5 degradation is also controlled by surface charge, adsorption, and radical formation. The response surface indicates that higher CDs doses and basic pH are advantageous for RB5 degradation, as expected for most heterogeneous photocatalytic reactions. Figure 12B illustrates the increase in RB5 degradation with increasing CD dose and its decrease with increasing initial RB5 concentration. The region with the highest predicted degradation is the high-dose/low-concentration region (0.8 g L^{-1} CDs and 10 mg L^{-1} RB5) under constant pH 7.4 and 75 min. The higher slope along the CDs dose axis suggests that catalyst dose has a greater impact, likely due to higher surface area and greater ROS formation.

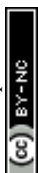
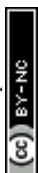
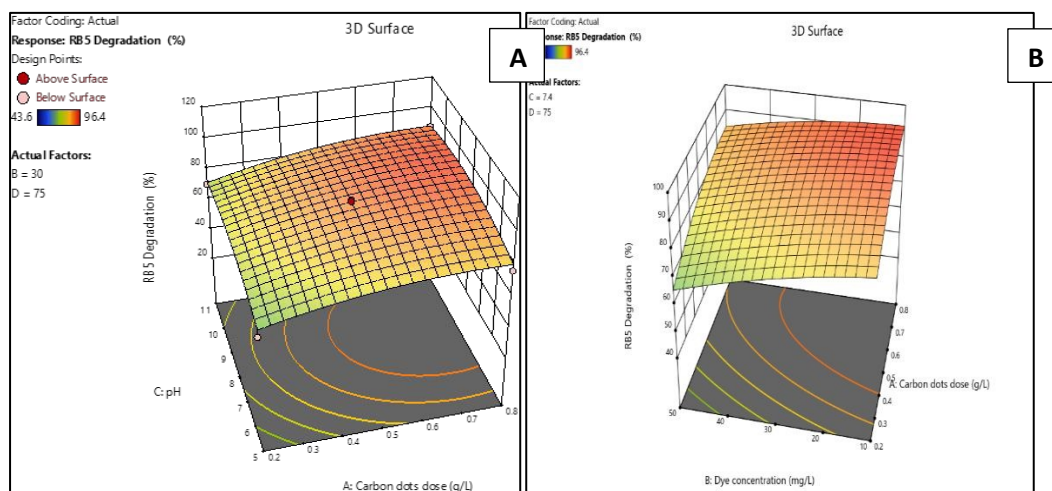
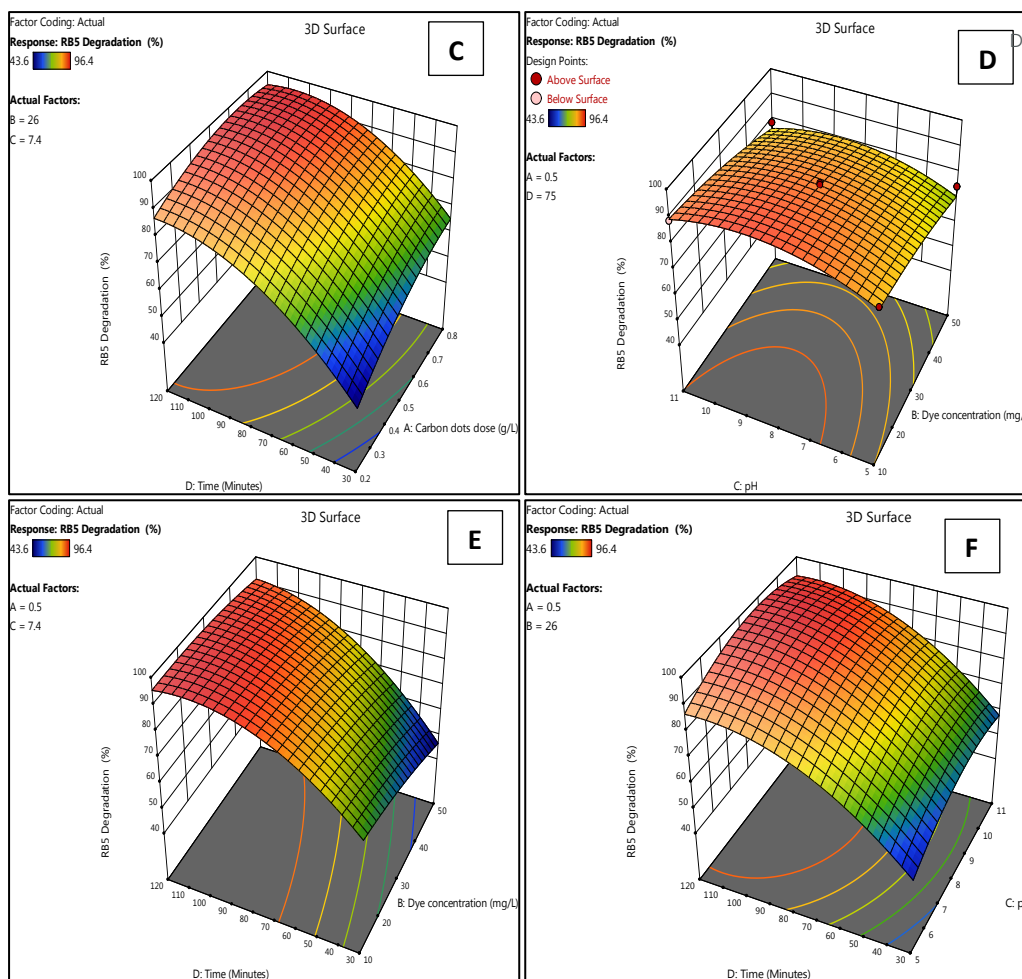


Figure 12C shows that RB5 degradation increases with the CDs dose and light exposure time. The response surface steadily increases with increasing dose and time, indicating a synergistic effect between the two parameters. The response surface suggests that the optimal degradation occurs at 0.8 g L^{-1} CDs and 120 min, with a fixed initial RB5 concentration (26 mg L^{-1}) and pH 7.4. In general, the graph confirms that increasing the catalyst amount and the light exposure time enhances RB5 degradation. The response surface in Figure 12D shows that the maximum RB5 degradation is predicted at slightly alkaline pH (9-10) and low initial RB5 concentration ($10\text{-}20 \text{ mg L}^{-1}$). It steadily decreases with increasing RB5 concentration and low pH.

The graph 12E indicates that RB5 degradation increases with irradiation time from 30 to 120 min, but decreases with increasing initial RB5 concentration from 10 to 50 mg L^{-1} . The highest degradation is obtained at low dye concentration (10 mg L^{-1}) and long irradiation time (120 min). However, at higher dye concentrations, around 50 mg L^{-1} , less degradation is observed, even at longer irradiation times. The RB5 degradation increases as the CDs dose rises from 0.2 to 0.8 g L^{-1} and exposure time increases from 30 to 120 min, as shown in Figure 12F. The highest degradation occurs at the highest CDs dose (0.8 g L^{-1}) and the longest irradiation time (120 min).





View Article Online
DOI: 10.1039/D6VA00121A

Figure 12: Three-dimensional response surface plots of the process variables on RBS degradation (%): (A) pH and activated carbon dose, (B) activated carbon dose and dye concentration, (C) time and activated carbon dose, (D) pH and dye concentration, (E) time and dye concentration, and (F) pH and time.



Table 3: Comparison of dye-degradation efficiency of the present CDs photocatalyst with other photocatalystsView Article Online
DOI: 10.1039/D6VA00121A

photocatalysts

Photocatalyst/system	Dye	Main conditions	Degradation efficiency	Reference
Carbon dots	RB 5	Optimized RSM conditions	96.4 (dark+ light)	PET-based carbon dots (current study)
Magnetic Nano catalyst	RB 5	pH 3, 20 mg L ⁻¹ RB5, 0.5 g L ⁻¹ catalyst, 120 min	99.99%	52
nZVI	RB 5	Solar irradiation, 120 min	90%	53
ZnO/UV slurry system	RB 5	pH 11, UV irradiation	Nearly 99%	54
TiO ₂ -based photocatalysis	RB 5	UV/TiO ₂ advanced oxidation process	77%	55

As shown in Figures S5 and S6 of supplementary file, the relative sensitivity plot and the diagnostic plots for the RB5 degradation model were obtained, which further support the importance of the selected factors as well as the fitted model. The quadratic polynomial equation in terms of coded factors for RB5 degradation is shown as follows:

$$\text{RB5 degradation(\%)} = 88.20 + 7.54A - 5.95B + 3.33C + 18.46D + 1.73AB + 0.7000AC - 3.05AD$$

3.3.11 Integration of RSM findings with pseudo-first-order kinetics

The RB5 degradation is modeled using the outputs in a pseudo-first-order (PFO) kinetic model by transforming the predicted degradation percentage into a fraction of the remaining concentration and subsequently into an apparent rate constant.

$$\text{Dye removal \%} = \frac{C_0 - C_t}{C_0} \times 100$$

According to the RSM outcomes the optimized degradation time is 75 minutes with 91.03% degradation.

$$\frac{C_t}{C_0} = 1 - \frac{\text{degradation}}{100} = 1 - 91.0375/100 = 0.0896$$



$$\ln \frac{C_t}{C_0} = \ln(1/\frac{C_t}{C_0}) = \ln 1/0.896 = 2.4121$$

View Article Online
DOI: 10.1039/D6VA00121A

With respect to pseudo-first-order model:

$$\ln \frac{C_t}{C_0} = k_{app} \times t$$

$$k_{app} = \frac{\ln \left(\frac{C_t}{C_0} \right)}{t} = \frac{2.4121}{75} = 0.03216 \text{ min}^{-1}$$

half-life: $t_{1/2} = \ln(2)/k_{app} = 0.6931/0.03216 = 21.6 \text{ min}$

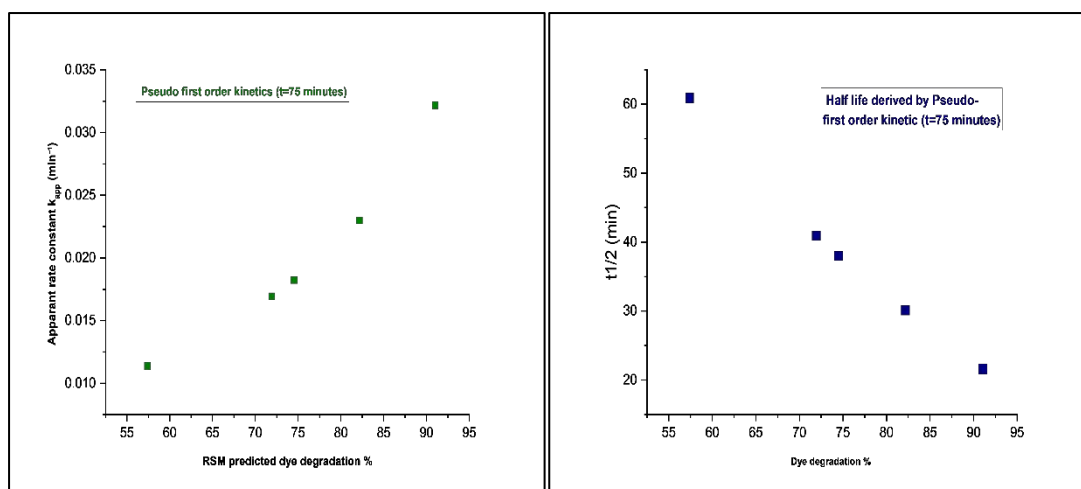


Figure 13: Pseudo-first-order kinetic trend of RB5 degradation for 75 min: fluctuation of k_{app} (left) and $t_{1/2}$ (right) predicted dye removal %.

RSM predicted ($t=75$ minutes) points were plotted to evaluate the kinetic trend of the data. the tabular data is presented in the supplementary file as Table S2, while the plots described in the Figure 13 demonstrate that dye degradation under the RSM predicted optimized conditions ($t = 75$ min) follows a pseudo-first-order reaction whereby the higher the degradation (%), the higher the apparent rate constant (k_{app}) and, consequently, the faster the reaction under the same conditions. The half-life ($t_{1/2}$) is also determined using the pseudo-first-order model, which decreases with increasing dye degradation, falling between approximately 60 and 20 minutes. In general, the greater the degradation, the larger k_{app} , and the shorter the $t_{1/2}$, indicating better kinetic performance and faster dye



degradation. The pseudo-first-order kinetic parameters and RSM model summary are presented in Tables S3 and S4 of the supplementary file. View Article Online
DOI:10.1039/D6VA00121A

3.3.12 RSM predicted data: Statistical evaluations

The ANOVA results revealed that the quadratic RSM model used to predict RB5 degradation was significant ($F = 46.63$, $p < 0.0001$), and model summary tables are given in the Supplementary Data as Table 6. The goodness of fit of the model was high ($R^2 = 0.9790$), and the adjusted $R^2 = 0.9580$ and the predicted $R^2 = 0.8799$. The model accuracy was reasonable as it was shown by low CV (3.98) and high Precision (23.38). There were significant linear effects of dose of carbon dots, concentration of dye used, pH and time (A, B, C and D respectively) and time (D) influenced the effect the most (F -value = 2.6). Among the terms of interaction, BD only turned out significant ($p = 0.0262$), which indicates the joint effect of dye concentration and time. The significance of quadratic terms A2 ($p = 0.0018$), C2 ($p < 0.0001$) and D2 ($p < 0.0001$) was significant, which indicated that the response surface was curvilinear. The significance of the lack-of-fit test ($p = 0.0014$) was high; thus, to test the model's assumptions, diagnostic plots were used to assess whether the residuals were randomly distributed.



Reusability potential of carbon dots

View Article Online
DOI: 10.1039/D6VA00121A

The reusability of the CDs photocatalyst showed that good photocatalytic degradation of RB5 could be achieved after five uses. The degradation efficiency slightly decreased with increasing number of cycles, due to surface fouling, small catalyst loss in the recovery process, or blockage of active sites by intermediate products⁵⁶. While the maintained efficiency after 5 cycles confirms satisfactory stability and reusability of CDs for the photocatalytic degradation of RB5 as shown in Figure 14. Photocatalytic activity slightly decreased after recycle runs could be attributed to small loss of catalyst during recovery and washing steps and partial coverage of active sites by adsorbed dye molecule or degradation intermediates, leaving fewer active sites and surface area for next cycles⁵⁷.

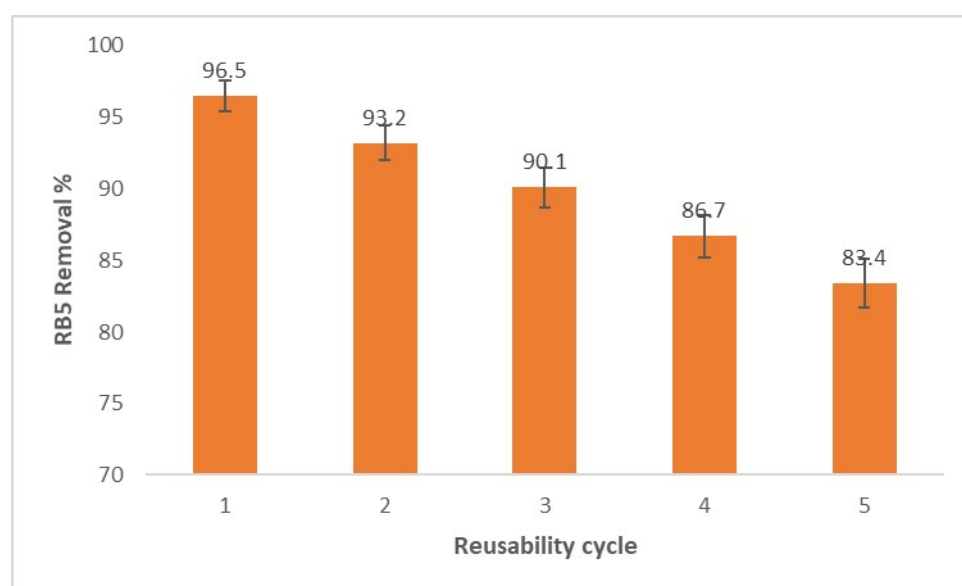
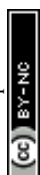


Figure 14: Reusability of CDs for five consecutive cycles

Conclusion

This research has shown the effective recycling of waste PET bottles to carbon dots (CDs) and their subsequent use as photocatalysts for Reactive Black 5 (RB5) dye removal. The CDs exhibited desirable optical and surface characteristics with a typical UV-vis absorption spectrum, blue photoluminescence emission, oxygen-/nitrogen-containing functional groups, nanoscale size and a rough surface, facilitating dye interaction and photocatalytic



activity. The RSM model identified optimal conditions for the dark adsorption/light photocatalytic process, which resulted in 96.5% removal of RB5. The RSM model demonstrated good predictability and revealed the significance of CDs dose, initial dye concentration, pH, and UV irradiation time on the degradation efficiency. The CDs were also found to be stable for recycling, with good performance over five cycles. In summary, this study offers an easy, eco-friendly, and waste-to-value approach for the sustainable treatment of dye-polluted water.

[View Article Online](#)

DOI: 10.2039/D6VA00121A

Author contributions

Seemab Javed is responsible for the conceptualization, methodology, investigation, data curation, and initial draft preparation. Shahzad Ali Shahid Chatha and Aman Ullah supervised the study, guiding its direction and methodology, and assisted with editing and manuscript review. Shafqat Ali oversaw the work and provided crucial input to review and improve the project analysis.

Conflicts of interest

There is no conflict of interest.

Data availability

All the generated data sets of the current study are available from the corresponding author on reasonable request

Acknowledgement

The author gratefully acknowledges the guidance and support of Dr. Aman Ullah, Dr. Shahzad Ali Shahid Chatha, and Dr. Shafaqat throughout the research process. Their supervision and feedback were crucial to this study. Additionally, the authors appreciate the support of the Department of Chemistry and the Department of Environmental Science



at Government College University, Faisalabad, and the Department of Agriculture, Food and Environmental Science, University of Alberta, Canada, for providing laboratory facilities and technical assistance in synthesizing and characterizing carbon dots from PET waste and their photocatalytic application.

References

1. A. M. Abdelfatah, M. Hosny, A. S. Elbay, N. El-Maghrabi and M. Fawzy, From Waste to Worth: Upcycling Plastic into High-Value Carbon-Based Nanomaterials, *Polymers*, 2024, **17**, 63.
2. M. Anwar, M. E. Konnova and S. Dastgir, Circular plastic economy for sustainable development: current advances and future perspectives, *RSC Sustainability*, 2025.
3. R. Vanaraj, S. M. Suresh Kumar, S. C. Kim and M. Santhamoorthy, A review on sustainable upcycling of plastic waste through depolymerization into high-value monomer, *Processes*, 2025, **13**, 2431.
4. J. Mehta, N. Dilbaghi, A. Deep, F. I. Hai, A. A. Hassan, A. Kaushik and S. Kumar, Plastic waste upcycling into carbon nanomaterials in circular economy: Synthesis, applications, and environmental aspects, *Carbon*, 2025, **234**, 119969.
5. X. Mu, Y. Li, X. Liu, C. Ma, H. Jiang, J. Zhu, X. Chen, T. Tang and E. Mijowska, Controllable carbonization of plastic waste into three-dimensional porous carbon nanosheets by combined catalyst for high performance capacitor, *Nanomaterials*, 2020, **10**, 1097.
6. Y. Wu, G. Ma, A. Zhang, W. Gu, J. Wei and R. Wang, Preparation of carbon dots with ultrahigh fluorescence quantum yield based on PET waste, *ACS omega*, 2022, **7**, 38037-38044.
7. W. Gu, Z. Dong, A. Zhang, T. Ma, Q. Hu, J. Wei and R. Wang, Functionalization of PET with carbon dots as copolymerizable flame retardants for the excellent smoke suppressants and mechanical properties, *Polymer Degradation and Stability*, 2022, **195**, 109766.
8. S. Chaudhary, M. Kumari, P. Chauhan and G. R. Chaudhary, Upcycling of plastic waste into fluorescent carbon dots: An environmentally viable transformation to biocompatible C-dots with potential prospective in analytical applications, *Waste Management*, 2021, **120**, 675-686.
9. C. Ma, G. Jin, P. He, C. Tang, L. Bing, B. Liu, H. Huang, Y. Fan, R. Wang and J. Wei, Optimization of preparation technology for PET-based Carbon Dots by response surface method and its application, *Journal of Fluorescence*, 2025, **35**, 6875-6885.
10. N. Eldomiaty, E. Elbayoumy, M. M. Aboelnga and M. R. Mostafa, Repurposing waste plastic into a sustainable adsorbent for removing synthetic dye: experimental, optimization and theoretical modeling, *RSC advances*, 2026, **16**, 1008-1029.
11. Y. Jiang, X. Zhang, L. Xiao, R. Yan, J. Xin, C. Yin, Y. Jia, Y. Zhao, C. Xiao and Z. Zhang, Preparation of dual-emission polyurethane/carbon dots thermoresponsive composite films for colorimetric temperature sensing, *Carbon*, 2020, **163**, 26-33.
12. Y. Iqbal, S. A. Shahid Chatha, I. Ahmed, K. Shahzad, M. Y. Siddique and U. Anwar, Moringa Gum-derived Polymeric Carbon Dots for Antimicrobial Activity, *BioResources*, 2025, **20**.
13. Y. Zhou, W. Zhang and R. M. Leblanc, Structure–property–activity relationships in carbon dots, *The Journal of Physical Chemistry B*, 2022, **126**, 10777-10796.



14. M. M. Islam, A. R. Aidid, J. N. Mohshin, H. Mondal, S. Ganguli and A. K. Chakraborty, A critical review on textile dye-containing wastewater: Ecotoxicity, health risks, and remediation strategies for environmental safety, *Cleaner Chemical Engineering*, 2025, **11**, 100165. View Article Online
DOI: 10.1039/D6VA00121A
15. M. K. A. Elnabi, M. A. Ghazy, S. S. Ali, M. Eltarahony and A. Nassrallah, Efficient biodegradation and detoxification of reactive black 5 using a newly constructed bacterial consortium, *Microbial Cell Factories*, 2025, **24**, 154.
16. S. Sadiq, S. A. S. Chatha, S. Ali, M. Shahid and P. K. Sarker, Microwave assisted synthesis of fly ash based zeolites for degradation of reactive blue 19 dye from wastewater, *Scientific Reports*, 2025, **15**, 16028.
17. H. A. Kiwaan, R. M. Basal, M. M. Aboelnga and M. R. Mostafa, Efficient photo-assisted degradation of wastewater dyes using CdS nanoparticles confined in porous G-C3N4/SiO2 composites, *Journal of Molecular Liquids*, 2023, **391**, 123301.
18. M. Magdy, M. M. Aboelnga and E. Elbayoumy, Sustainable removal of brilliant green dye from aqueous media using a calcium alginate–polydopamine bio-composite: process optimization and adsorption mechanism, *Materials Advances*, 2026, **7**, 2785-2802.
19. S. S. Makgato, Analysis of municipal solid waste in Soweto, Johannesburg Municipality, South Africa: Implications for sustainable waste management practices, *Chemical Engineering Transactions*, 2024, **109**, 37-42.
20. A. M. Parambil and P. Rajamani, Carbon dots: a promising path towards environmental sustainability, *Environmental Science: Advances*, 2024, **3**, 1513-1523.
21. A. D. Ambaye, T. G. Kebede, N. Raleie, S. Dube, M. Mathe, M. M. Nindi, S. Makgato and T. Mokrani, Recent advances in carbon dot-driven nanomaterials for photoelectrochemical-based degradation of contaminants: A Review, *International Journal of Electrochemical Science*, 2026, 101297.
22. K. F. Kayani, S. J. Mohammed, M. S. Mustafa and S. B. Aziz, Dyes and their toxicity: removal from wastewater using carbon dots/metal oxides as hybrid materials: a review, *Materials Advances*, 2025, **6**, 5391-5409.
23. L. Buenaño, E. Ali, A. Jafer, S. H. Zaki, F. J. Hammady, S. B. Khayoun Alsaadi, M. M. Karim, M. F. Ramadan, A. A. Omran and A. Alawadi, Optimization by Box–Behnken design for environmental contaminants removal using magnetic nanocomposite, *Scientific Reports*, 2024, **14**, 6950.
24. M. Hussain, A. Abbas, T. Ahmad, S. Ullah, S. Chatha and T. Shifa, Na-alginate coated waste banana-derived biochar composite for heavy metals removal and parametric optimization using RSM–CCD model, *International Journal of Environmental Science and Technology*, 2026, **23**, 159.
25. X. Zhou, J. Deng, Z. Li, Y. Cheng, J. Zhou, M. Jiang and W. Dong, One-Pot Synthesis of Multicolor Carbon Dots from PET Plastic Waste for White Light-Emitting Diodes, *ACS Sustainable Chemistry & Engineering*, 2024, **12**, 16592-16602.
26. I.-H. Tsai, J.-T. Li and C.-W. Chang, Effects of sonication and hydrothermal treatments on the optical and chemical properties of carbon dots, *ACS omega*, 2021, **6**, 14174-14181.
27. L. Cao, J. Li, Y. Song, S. Cong, H. Wang and M. Tan, Molecular interaction of fluorescent carbon dots from mature vinegar with human hemoglobin: Insights from spectroscopy, thermodynamics and AFM, *International journal of biological macromolecules*, 2021, **167**, 415-422.
28. D.-K. Lee, S. Jeon, J. Jeong, K. S. Song and W.-S. Cho, Carbon nanomaterial-derived lung burden analysis using UV-Vis spectrophotometry and proteinase K digestion, *Particle and fibre toxicology*, 2020, **17**, 43.
29. Y. Wu, R. Wang, W. Xie, G. Ma, A. Zhang, B. Liu, H. Huang, L. Gao, M. Qu and Y. Wei, Solvent-thermal preparation of sulfur and nitrogen-doped carbon dots with PET waste as



precursor and application in light-blocking film, *Journal of Nanoparticle Research*, 2023, **25**, 18. Open Access Article Online
DOI: 10.1039/C6VA00121A

30. J. Jiang, G. Ye, Z. Wang, Y. Lu, J. Chen and K. Matyjaszewski, Heteroatom-Doped Carbon Dots (CDs) as a Class of Metal-Free Photocatalysts for PET-RAFT Polymerization under Visible Light and Sunlight, *Angewandte Chemie*, 2018, **130**, 12213-12218.
31. P. Roy, P.-C. Chen, A. P. Periasamy, Y.-N. Chen and H.-T. Chang, Photoluminescent carbon nanodots: synthesis, physicochemical properties and analytical applications, *Materials Today*, 2015, **18**, 447-458.
32. W. K. Szapoczka, A. L. Truskewycz, T. Skodvin, B. Holst and P. J. Thomas, Fluorescence intensity and fluorescence lifetime measurements of various carbon dots as a function of pH, *Scientific Reports*, 2023, **13**, 10660.
33. C. Liu, F. Zhang, J. Hu, W. Gao and M. Zhang, A mini review on pH-sensitive photoluminescence in carbon nanodots, *Frontiers in chemistry*, 2021, **8**, 605028.
34. Arpita, P. Kumar, N. Kataria, N. Narwal, S. Kumar, R. Kumar, K. S. Khoo and P. L. Show, Plastic waste-derived carbon dots: insights of recycling valuable materials towards environmental sustainability, *Current pollution reports*, 2023, **9**, 433-453.
35. Z. Chen, Y. Liu and Z. Kang, Diversity and tailorability of photoelectrochemical properties of carbon dots, *Accounts of Chemical Research*, 2022, **55**, 3110-3124.
36. N. A. Lynd, A. J. Meuler and M. A. Hillmyer, Polydispersity and block copolymer self-assembly, *Progress in Polymer Science*, 2008, **33**, 875-893.
37. Z. Jia, J. Li, L. Gao, D. Yang and A. Kanaev, Dynamic light scattering: a powerful tool for in situ nanoparticle sizing, *Colloids and Interfaces*, 2023, **7**, 15.
38. J. Rodriguez-Loya, M. Lerma and J. L. Gardea-Torresdey, Dynamic light scattering and its application to control nanoparticle aggregation in colloidal systems: a review, *Micromachines*, 2023, **15**, 24.
39. M. Egorova, A. Tomskaya and S. A. Smagulova, Optical properties of carbon dots synthesized by the hydrothermal method, *Materials*, 2023, **16**, 4018.
40. C. M. Singaravelu, X. Deschanel, C. Rey and J. Cause, Investigation on Fluorescence Origin and Spectral Heterogeneity in Carbon Dots: A Dynamic Perspective, *ChemPhotoChem*, 2024, **8**, e202400044.
41. P. F. Andrade, G. Nakazato and N. Durán, 2017.
42. J. Ren, F. Weber, F. Weigert, Y. Wang, S. Choudhury, J. Xiao, I. Lauer mann, U. Resch-Genger, A. Bande and T. Petit, Influence of surface chemistry on optical, chemical and electronic properties of blue luminescent carbon dots, *Nanoscale*, 2019, **11**, 2056-2064.
43. K. J. Mintz, M. Bartoli, M. Rovere, Y. Zhou, S. D. Hettiarachchi, S. Paudyal, J. Chen, J. B. Domena, P. Y. Liyanage and R. Sampson, A deep investigation into the structure of carbon dots, *Carbon*, 2021, **173**, 433-447.
44. A. Kelarakis, From highly graphitic to amorphous carbon dots: A critical review, *MRS Energy & Sustainability*, 2014, **1**, E2.
45. P. Ma, J. Zuo, Z. Li, D. Xiao, H. Wu, Y. Zhang and A. Dong, Application progress of green carbon dots in analysis and detection, *Particle & Particle Systems Characterization*, 2022, **39**, 2200104.
46. Y. Chen, X. Zhu, H. Liu and B. Sun, Synergistic PET/IFE-driven fluorescence-phosphorescence dual signal quenching in RTP CDs sensor for sensitive thiram monitoring in food safety, *Microchimica Acta*, 2025, **192**, 1-10.
47. M. Aasadnia, M. Mehrpooya and B. Ghorbani, A novel integrated structure for hydrogen purification using the cryogenic method, *Journal of Cleaner Production*, 2021, **278**, 123872.
48. B. D. Mansuriya and Z. Altintas, Carbon dots: classification, properties, synthesis, characterization, and applications in health care—an updated review (2018–2021), *Nanomaterials*, 2021, **11**, 2525.



49. J. Feng, X. Ran, L. Wang, B. Xiao, L. Lei, J. Zhu, Z. Liu, X. Xi, G. Feng and Z. Dai, The synergistic effect of adsorption-photocatalysis for removal of organic pollutants on mesoporous Cu₂V₂O₇/Cu₃V₂O₈/g-C₃N₄ heterojunction, *International Journal of Molecular Sciences*, 2022, **23**, 14264. View Article Online
DOI: 10.1039/D6VA00121A
50. S. Tak, S. Grewal, Shreya, P. Phogat, Manisha, R. Jha and S. Singh, Mechanistic insights and emerging trends in photocatalytic dye degradation for wastewater treatment, *Chemical Engineering & Technology*, 2024, **47**, e202400142.
51. S. Khan, T. Noor, N. Iqbal and L. Yaqoob, Photocatalytic dye degradation from textile wastewater: a review, *ACS omega*, 2024, **9**, 21751-21767.
52. M. Mohammadi-Galangash, S.-K. Mousavi and M. Shirzad-Siboni, Photocatalytic degradation of reactive black 5 from synthetic and real wastewater under visible light with TiO₂ coated PET photocatalysts, *Scientific Reports*, 2025, **15**, 14314.
53. H. Nassehinia, H. Rahmani, K. Rahmani and A. Rahmani, Solar photocatalytic degradation of Reactive Black 5: by-products, bio-toxicity, and kinetic study, *Desalination and Water Treatment*, 2020, **206**, 385-395.
54. S. Laohaprapanon, J. Matahum, L. Tayo and S.-J. You, Photodegradation of reactive black 5 in a ZnO/UV slurry membrane reactor, *Journal of the Taiwan Institute of Chemical Engineers*, 2015, **49**, 136-141.
55. E. Kusvuran, S. Irmak, H. I. Yavuz, A. Samil and O. Erbatur, Comparison of the treatment methods efficiency for decolorization and mineralization of Reactive Black 5 azo dye, *Journal of Hazardous Materials*, 2005, **119**, 109-116.
56. K. J. Amaya-Galván, K. J. Ramírez-Escárcega, F. L. Zaruma-Torres, F. d. J. Silerio-Vazquez and J. B. Proal-Nájera, Pharmaceutical pollutants in water: Carbon nanotube–photocatalyst composites as a path forward, *Journal of Environmental Chemical Engineering*, 2025, **13**, 115086.
57. P. Gharbani, A. Mehrizad and S. A. Mosavi, Optimization, kinetics and thermodynamics studies for photocatalytic degradation of Methylene Blue using cadmium selenide nanoparticles, *npj Clean Water*, 2022, **5**, 34.



Data Availability

The data supporting the findings of this study are available from the corresponding author upon reasonable request.

